Accepted Manuscript

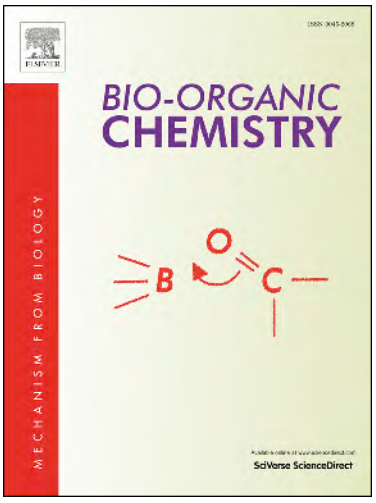

Discovery of Novel Quinazolines as Potential Anti-tubulin Agents Occupying Three Zones of Colchicine domain

Wenlong Li, Ying Yin, Wen Shuai, Feijie Xu, Hong Yao, Jie Liu, Keguang Cheng, Jinyi Xu, Zheying Zhu, Shengtao Xu

PII: S0045-2068(18)30618-7
DOI: https://doi.org/10.1016/j.bioorg.2018.10.027
Reference: YBIOO 2561

To appear in: *Bioorganic Chemistry*

Received Date: 23 June 2018
Revised Date: 10 October 2018
Accepted Date: 15 October 2018

Please cite this article as: W. Li, Y. Yin, W. Shuai, F. Xu, H. Yao, J. Liu, K. Cheng, J. Xu, Z. Zhu, S. Xu, Discovery of Novel Quinazolines as Potential Anti-tubulin Agents Occupying Three Zones of Colchicine domain, *Bioorganic Chemistry* (2018), doi: https://doi.org/10.1016/j.bioorg.2018.10.027

Discovery of Novel Quinazolines as Potential Anti-tubulin Agents Occupying Three Zones of Colchicine domain

Wenlong Li[a], Ying Yin[a], Wen Shuai[a], Feijie Xu[a], Hong Yao[a], Jie Liu[b, c], Keguang Cheng[c], Jinyi Xu[a, *], Zheying Zhu[d, *], Shengtao Xu[a, *]

[a]State Key Laboratory of Natural Medicines and Department of Medicinal Chemistry, China Pharmaceutical University, 24 Tong Jia Xiang, Nanjing 210009, P. R. China

[b]Department of Organic Chemistry, China Pharmaceutical University, 24 Tong Jia Xiang, Nanjing 210009, P. R. China

[c]State Key Laboratory for the Chemistry and Molecular Engineering of Medicinal Resources, and School of Chemistry and Pharmacy, Guangxi Normal University, Guilin 541004, China

[d]Division of Molecular Therapeutics & Formulation, School of Pharmacy, The University of Nottingham, University Park Campus, Nottingham NG7 2RD, UK

[*]**Corresponding authors:** jinyixu@china.com (J. Xu); Zheying.Zhu@nottingham.ac.uk (Z. Zhu); cpuxst@163.com (S. Xu).

Abstract

A series of novel quinazolines as tubulin inhibitors occupying three zones of colchicine domain have been designed and synthesized inspired by the recently disclosed crystal structure of verubulin analogue **6** with tubulin. Among the newly synthesized compounds, **19c** showed noteworthy potency against K562, HepG2, KB, HCT-8 and MDB-MB-231 cancer cells. *In vitro* microtubule polymerization assays identified **19c** as a potent tubulin assembly inhibitor, the binding mode of which with tubulin was confirmed by molecular modelling studies to occupy three zones of tubulin domain. Furthermore, **19c** disrupted the intracellular microtubule network, caused G2/M phase arrest, induced cell apoptosis and depolarized mitochondria of K562 cells. **19c** also reduced the cell migration and disrupted the capillary-like tube formation of human umbilical vein endothelial cells (HUVECs). Importantly, **19c** significantly and dose dependently inhibited tumor growth in H22 liver cancer xenograft mouse model. All these results suggested that **19c** deserves further research as a novel and potential anti-tubulin agent for the treatment of cancers.

Key words: microtubule; tubulin inhibitor; colchicine domain; anti-vascular; anti-

tumor

1. Introduction

Microtubules are ubiquitous cellular polymers that play diverse roles within the cell, such as maintenance of cell structure, protein trafficking, chromosomal segregation, and mitosis [1]. Microtubules are long and hollow structures with 5 nm walls surrounding a cavity, and are made up of two globular protein subunits, α- and β-tubulin [2-4]. Microtubule-targeting agents (MTAs) that stabilize or destabilize microtubule can interfere with microtubule dynamics, which leads to mitotic block and cell apoptosis. MTAs are divided into two classes including microtubule destabilizing agents and microtubule stabilizing agents [5]. At least three binding sites in tubulin including taxane, vinca alkaloid and colchicine binding sites, have been identified, which can be interfered by MTAs. The compounds targeting taxane binding site stabilize microtubule, while those targeting vinca alkaloid and colchicine binding sites destabilize microtubules [6]. Inhibitors that target colchicine binding site are characterized with many advantages compared with those binding another two sites, such as simpler structures, improved aqueous solubility, reduced toxicity and multidrug resistance (MDR) effects. Notably, the colchicine-site binders also exhibit antiangiogenic and vascular disrupting activities which are not found in other site binders [7]. Extensive efforts have been made to develop colchicine binding site inhibitors (CBSIs) either from natural products or synthetic origins, and several candidates are under clinical investigations as potential novel anti-cancer agents [8, 9].

Colchicine-binding domain is a deep pocket located at the α-β interface of tubulin heterodimers, which comprises a main site (colchicine binding site) and an additional neighboring pocket [10]. The colchicine domain can be divided into three zones including zones 1, 2 and 3 [11, 12]. Classical CBSIs are featured with an "aromatic ring - bridge - aromatic ring" structure character exemplified by colchicine (**1**) and combretastatin A-4 (**2**, CA-4) (Figure 1), and they mostly have globular or butterfly-like shape forming a specific spatial conformation in which ring A and ring B occupy zone 2 and zone 1 of the colchicine domain, respectively. CBSIs that simultaneously occupy three zones in the cavity have been rarely reported.

ABT-751 (**3**), also named E7010, was a potent anti-proliferative agent firstly found in 1992 [13] and was subsequently identified to target the colchicine site of tubulin [14]. In 2009, the crystal structure of ABT-751 with tubulin was obtained and it showed that ABT-751 was buried more deeply than colchicine and occupied three zones of colchicine domain at the same time. The 4-methoylphenyl of ABT-751 is accommodated into zone 1 with pyridine ring in zone 2, and the phenol extends into the deeper site of β-tubulin, namely zone 3, forming hydrogen bond with Tyrβ202 residue [10]. Another reported compound that occupied all three zones of colchicine domain was

4 whose *m*-ethoxyaniline group was extended into zone 3 of colchicine domain and formed hydrogen bond with Tyrβ202 [15]. Several residues in zone 2 and zone 3 differ among the β tubulin isotypes, which may provide opportunities to improve the selectivity of CBSIs to the isotype α β III tubulin isoform that is commonly overexpressed in cancer cells [16,17]. Thus, the above-mentioned CBSIs with unique binding poses may be conferred with specific targeting to tubulin isotypes, thereby lowering general toxicity.

Verubulin (**5**) was a potent tubulin polymerization inhibitor targeting the colchicine binding site, and demonstrated low nanomolar potency against diverse cancer cell lines [18, 19]. Verubulin had entered into clinical trials for patients with advanced cancer [20], but had been discontinued due to cardiovascular toxicity revealed in phase I and phase II studies [21]. The binding mode of verubulin with tubulin was yet unknown until the crystal structure of tubulin in complex with verubulin analogue **6** was determined recently [22]. Surprisingly, the binding pose of **6** is flipped over 180° compared to the published molecular modeling [23, 24]. The rings A and B of compound **6** occupied zone 2, and the rings C and D extended into zone 1 (Figure 2). The *N* atom at the 1-position of ring B interacted with the residue Cys241 via a water-mediated hydrogen bond. The chlorine atom at 2-position of ring B pointed to the deep pocket of *β*-tubulin, namely zone 3, reminding us that the position 2 of quinazoline may tolerate derivatization to extend into zone 3, thus the novel CBSIs occupy all the three zones of colchicine domain could be deigned. Inspired by the binding mode of ABT-751 with tubulin, various substituted phenyl moieties that might form hydrogen bond with Tyrβ202 residue were introduced to the C2-position of quinazoline skeleton of verubulin (Figure 2). Herein, we wish to report the synthesis and biological studies of these novel quinazoline derivatives as tubulin inhibitors occupying three zones of colchicine domain.

Figure 1. Representative tubulin inhibitors targeting colchicine binding site. Pink represents moieties occupying zone 1, red represents moieties occupying zone 2 and blue represents moieties extending into zone 3.

Figure 2. The rational design of quinazolines as tubulin inhibitors occupying three zones of colchicine domain.

2 Results and discussion

2.1 Chemistry

Key intermediate 4-oxo-3,4-dihydroquinazoline-2-carboxylic acid ethyl ester (**9**) was synthesized via a two-step acylation/cyclization sequence using anthranilamide (**7**) as the starting material according to the literature report [25] (Scheme 1). Following chlorination of **9** using $POCl_3$ afforded **10** which underwent a nucleophilic addition with *N*-methyl-4-methoxyaniline to give intermediate **11**. Quinazoline-2-carboxylic acid (**12**) was obtained by esterolysis of **11**, following condensation reactions with various anilines produced compounds **13a-c**, and further deprotection of **13b** gave compound **13d**.

Scheme 2 outlines the synthesis route of compounds **19a-t**. The key intermediate 2,4-dichloroquinazoline (**17**) was synthesized according to the literature report [26]. The starting material 2-amino-1-methyl benzoate (**14**) was coupled with KCNO in acetic acid at ambient temperature. Cyclization of methyl 2-ureidobenzoate (**15**) was processed in KOH methanol solution (pH = 10) at reflux temperature to produce **16**. 2,4-Dichloroquinazoline (**17**) was then achieved by refluxing **16** with $POCl_3$ in the presence of DIPEA in toluene. Then, *N*-methyl-4-methoxyaniline was attached to the 4-position of 2,4-dichloroquinazoline (**17**) through nucleophilic addition under basic condition in THF at room temperature to form intermediate **18**. Another nucleophilic addition with various anilines or benzylamines under EtOH in sealed tube at 150 ℃ produced compounds **19a-t**, and **19e** was further deprotected to produce compound **19f**.

Scheme 1. Synthesis of compounds **13a-d**[a].

[a]Reagents and conditions: (a) Et_3N, THF, 0 °C to rt; (b) $NaOCH_3$, EtOH, 0 °C to rt; (c) $POCl_3$, DIPEA, toluene, reflux; (d) *N*-methyl-4-methoxyaniline, concentrated HCl, isopropanol, rt; (e) 10% NaOH aqueous, CH_3OH, reflux; (f) various anilines, Et_3N, HATU, CH_3CN, rt; (g) TBAF, THF, rt.

Scheme 2. Synthesis of compounds **19a-t**[a].

[a]Reagents and conditions: (a) KNCO, AcOH, H_2O, rt; (b) KOH, CH_3OH, H_2O, reflux; (c) $POCl_3$, DIPEA, toluene, reflux; (d) *N*-methyl-4-methoxyaniline, Et_3N, THF, rt; (e) various anilines or

benzylamines, EtOH, 150 ℃, sealed tube; (f) TBAF, THF, rt.

2.2 *In vitro anti-proliferative and anti-tubulin activity*

The effect of linkers attached to the 2-position of quinazoline on anti-proliferative activity was firstly investigated. Eight compounds **13a**, **13c**, **13d**, **19a**, **19b** and **19f-h** bearing three kinds of linkers including amide bond, amino and aminomethyl were screened for their anti-proliferative activities in human leukemia cell lines (K562) by MTT assays. The results showed that compounds bearing amide bond (**13a**, **13c**, **13d**) and amino (**19a, 19g**) exhibited no obvious cytotoxicity at both 1 μM and 0.1 μM concentrations except **19f** which had an inhibitive rate of 87.6% at 1 μM. However, compounds with aminomethyl as the linker (**19b**, **19h**) exhibited significant cytotoxicity with the inhibitive rates of 95.3% and 80.5%, respectively at 1 μM concentration (see supporting information S1). Thus, aminomethyl was identified as the best linker that could orient additional phenyl moieties to zone 3 and was used for the next derivatization.

Seventeen compounds **19b-d, 19f** and **19h-t** were further evaluated for their anti-proliferative activities by MTT assays using the typical tubulin inhibitor ABT-751 that occupies three zones of colchicine domain as the positive control. Various hydrogen bond acceptors were introduced to the methylamino linker with the wish that they may form hydrogen bonds with the Tyrβ202 residue in zone 3, resembling the interaction of phenolic hydroxyl of ABT-751. As shown in Table 1, most of the compounds exhibited potent anti-proliferative activities. Substitutions at the 3-position of the phenyl moiety (**19c**, **19n**) seem to be favorable for the improvement of activity, compound **19c** bearing 3-pyridine (IC_{50} = 0.10 μM) and compound **19n** bearing 3-methoylphenyl (IC_{50} = 0.13 μM) were about 25 folds more potent than ABT-751 (IC_{50} = 2.82 μM). The effect of substitutions at the linker on activity was also investigated, either the *N*-CH_3 linker (**19r**) or tetrahydroisoquinoline linker (**19t**) led to the dramatically loss of activity while the methyl substitution at the methylene position (**19s**) maintained the activity.

Four representative compounds **19b**, **19c, 19h** and **19n** were chosen to evaluate their anti-proliferative activities against another four cancer cell lines including HepG2, KB, HCT-8 and MDA-MB-231 (Table 2). Interestingly, **19n** was less sensitive against these four cancer cell lines than K562 cells with the IC_{50} values ranging from 0.74 to 1.17 μM, while **19c** displayed no obvious selectivity among these four cancer cell lines with the IC_{50} values ranging from 0.11 to 0.13 μM, which was about 50 folds more potent than ABT-751.

In vitro tubulin polymerization inhibition assays further demonstrated that **19b**, **19c**, **19h** and **19n** were potent tubulin polymerization inhibitors. Among them, **19c** (IC_{50} = 2.45 μM) and **19h** (IC_{50} = 2.67 μM) were comparable with ABT-751 (IC_{50} = 2.24 μM)

(Table 2). Considering the good performance of **19c** in both *in vitro* anti-proliferative assays and *in vitro* tubulin polymerization inhibition assays, it was selected for further biological studies.

Table 1. Anti-proliferative activities of compounds against K562 cell line[a].

Compd.	IC_{50} values (μM)[b]	Compd.	IC_{50} values (μM)[b]
	K562		K562
19b	0.24±0.04	**19m**	0.37±0.02
19c	**0.10±0.01**	**19n**	**0.13±0.01**
19d	0.63±0.04	**19o**	0.56±0.02
19f	0.33±0.02	**19p**	0.41±0.02
19h	0.28±0.03	**19q**	0.85±0.05
19i	0.38±0.02	**19r**	>5
19j	0.31±0.03	**19s**	0.65±0.03
19k	0.31±0.02	**19t**	>5
19l	0.43±0.03	ABT-751	2.82±0.10

[a] Cells were treated with different concentrations of the compounds for 72 h. Cell viability was measured by the MTT assay as described in the Experimental Section.

[b] IC_{50} values are indicated as the mean ± SD (standard error) of at least three independent experiments.

Table 2. Anti-proliferative activities against four cancer cell lines [a], and ITP of compounds **19b**, **19c, 19h**, **19n** and ABT-751.

Compd.	IC_{50} values (μM)[b]				
	HepG2	KB	HCT-8	MDA-MB-231	ITP[c]
19b	0.58±0.05	0.48±0.04	0.47±0.03	0.46±0.03	5.29±0.25
19c	0.11±0.01	0.11±0.02	0.13±0.01	0.12±0.01	2.45±0.16
19h	0.21±0.02	0.37±0.03	0.48±0.01	0.47±0.05	2.67±0.18
19n	0.74±0.02	1.11±0.05	1.17±0.07	1.08±0.06	5.56±0.28
ABT-751	5.94±0.51	5.32±0.32	5.78±0.65	4.73±0.43	2.24±0.13

[a] Cells were treated with different concentrations of the compounds for 72 h. Cell viability was measured by the MTT assay as described in the Experimental Section.

[b] IC_{50} values are indicated as the mean ± SD (standard error) of at least three independent experiments.

[c] Inhibition of tubulin polymerization activity.

2.3 Molecular modeling

To validate whether **19c** would occupy three zones of colchicine domain as ABT-751, molecular modeling studies were performed. ABT-751 was firstly redocked into the colchicine domain resulting a similar conformation to that of ABT-751 in the crystal

structure with the root mean square deviation (RMSD) value of 0.93 (PDB code: 3HKC), which indicated the feasibility of our docking method. The docking results of **19c** displayed that it occupied three zones of colchicine domain in a similar positioning of ABT-751 (Figure 3A). The 4-meothylphenyl moiety of **19c** located in zone 1 that was surrounded by residues Thr314, Lys352 and Asn258, and the quinazoline occupied in zone 2 with the 1-*N* forming a critical hydrogen bond with residue Cys241. 3-Pyridine moiety extended into the deep pocket and was fixed by the hydrogen bond between *N* atom of pyridine and residue Tyr202. Verubulin was also docked into the protein which indicated that it adopted the similar location with that of verubulin **6** in the crystal structure (PDB code: 4I55), and 1-*N* formed a critical hydrogen bond with residue Cys241 (Figure 3B). The quinazoline moiety of **19c** was highly overlapped with verubulin in the colchicine domain with the additional 3-pyridine moiety extended into zone 3. All these docking results demonstrated that **19c** was a colchicine binding site inhibitor with a unique binding mode that it occupies three zones of colchicine domain.

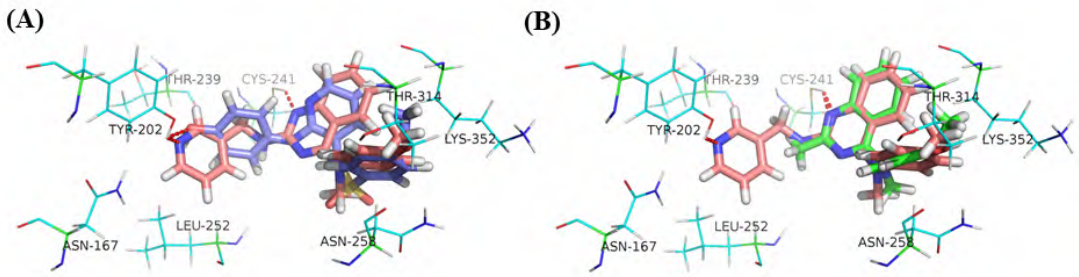

Figure 3. Proposed binding models for representative compounds binding with tubulin (PDB code: 3HKC) (A) ABT-751 (shown in blue) and **19c** (shown in pink); (B) verubulin (shown in green) and **19c** (shown in pink).

*2.4 Anti-microtubule effect of **19c** in K562 cells*

Immunofluorescent assay was performed to investigate the effect of compound **19c** on microtubule networks (Figure 4). Vehicle treated K562 cells exhibited normal filamentous microtubules arrays. However, when treated with **19c** at three different concentrations (0.05 μM, 0.10 μM, and 0.20 μM) for 24 h, the microtubule networks in cytosol were disrupted; these results indicated that **19c** can induce a dose-dependent collapse of the microtubule networks.

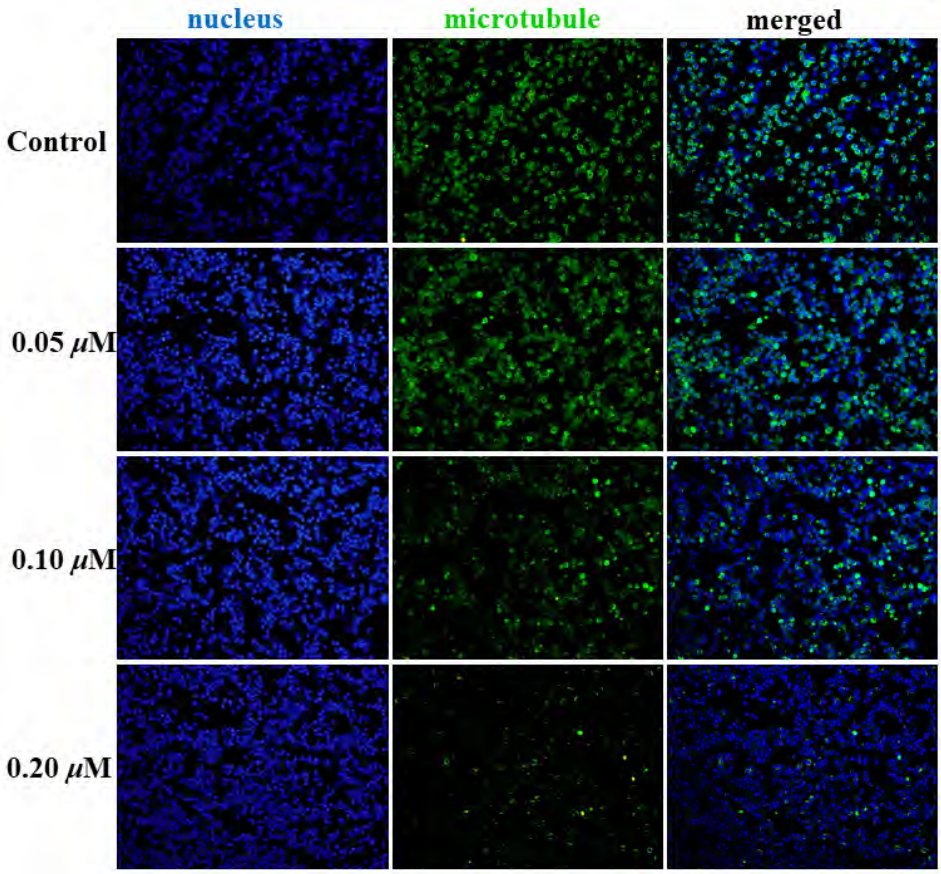

Figure 4. Effects of compound **19c** on the cellular microtubule networks visualized by immunofluorescence. K562 cells were treated with vehicle control 0.1% DMSO, **19c** (0.05 μM, 0.1 μM, and 0.2 μM). Then, the cells were fixed and stained with anti-α-tubulin-FITC antibody (green), Alexa Fluor 488 dye and counterstained with DAPI (blue).

2.5 Cell cycle analysis

Most microtubule polymerization inhibitors alter the tubulin-microtubule equilibrium, causing mitotic arrest at G2/M phase and ultimately apoptotic cell death. Thus, the most active compound **19c** was examined for its effect on cell cycle progression of K562 cells using propidiumiodide (PI) staining by flow cytometry analysis. As depicted in Figure 5, treatment with compound **19c** resulted in a gradual accumulation of cells in the G2/M phase of cell cycle in a dose-dependent manner. The percentages of cells arrested at the G2/M phase increased from 15.82% to 22.86%, 25.72%, and 27.67% at concentrations of 0, 0.05, 0.1, and 0.2 μM, respectively. These results demonstrated that **19c** can induce cell cycle arrest at G2/M phase.

2.6 Cell apoptosis analysis

The effects of **19c** on K562 cell apoptosis were further evaluated in Annexin V-FITC and propidium iodide (PI) staining assays and analyzed by flow cytometry (Figure 6).

The percentage of apoptotic cells after 48 h treatment was only 5.74% in the control group. However, the total numbers of early (Annexin -V^+/PI^-) and late (Annexin-V^+/PI^+) apoptotic cells increased to 19.8%, 37.4% and 65.0% after treatment with **19c** at 0.05, 0.1, and 0.2 μM for 48 h, respectively. These results confirmed that **19c** effectively induced cell apoptosis in K562 cells in a dose-dependent manner.

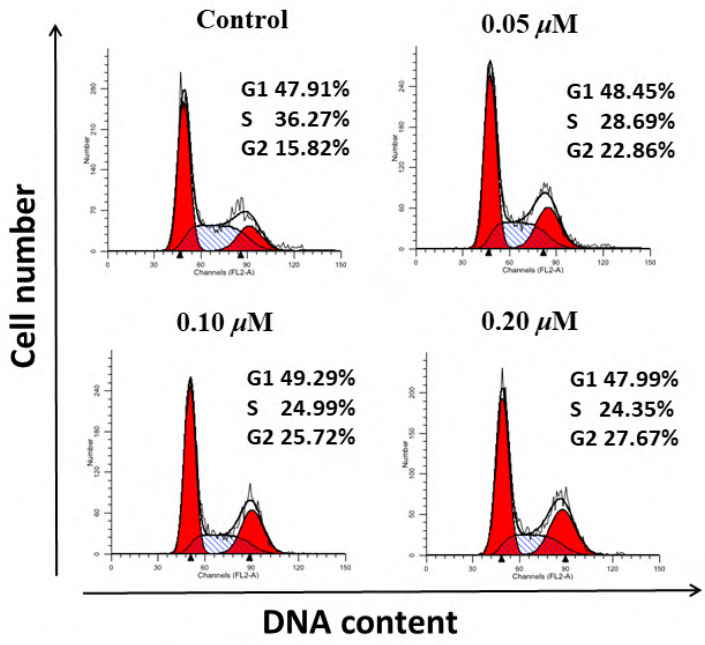

Figure 5. Compound **19c** induced G2/M arrest in K562 cells. K562 cells were incubated with varying concentrations of **19c** (0, 0.05, 0.1, and 0.2 μM) for 48 h. Cells were harvested and stained with PI and then analyzed by flow cytometry. The percentages of cells in different phases of cell cycle were analyzed by ModFit 4.1.

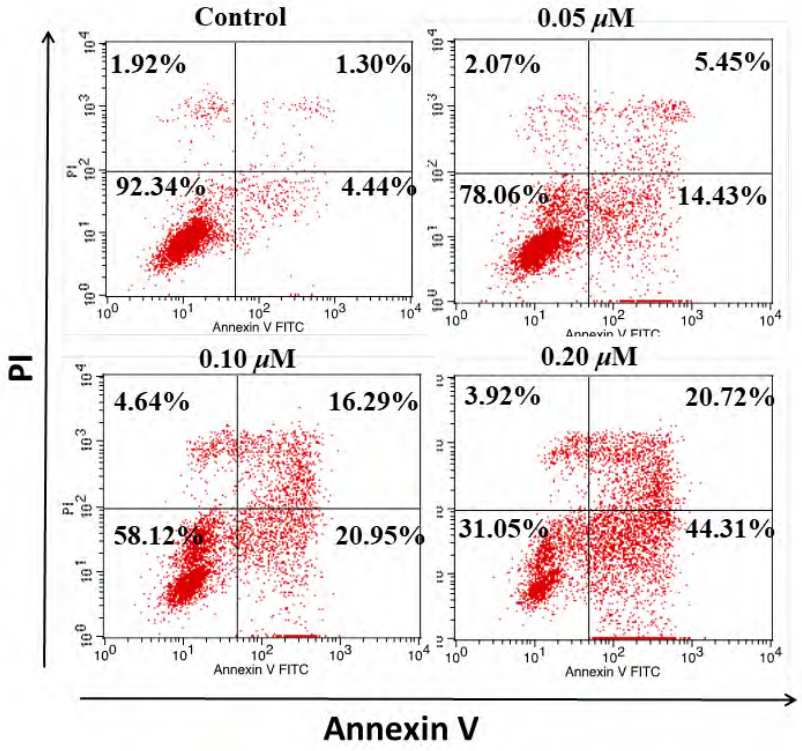

Figure 6. Compound **19c** induced apoptosis in K562 cells. K562 cells were incubated with varying concentrations of **19c** (0, 0.05, 0.1, and 0.2 μM). After 48 h of incubation, cells were collected and stained with Annexin-V/PI, followed by flow cytometric analysis. The percentages of cells in each stage of cell apoptosis were quantified by flow cytometry: (upper left quadrant) necrosis cells; (upper right quadrant) late-apoptotic cells; (bottom left quadrant) live cells; and (bottom right quadrant) early apoptotic cells.

2.7 Mitochondrial membrane potential (MMP) analysis

In order to determine whether **19c**-induced apoptosis was involved in a disruption of mitochondrial membrane integrity, the fluorescent probe JC-1 was employed to measure the MMP (Figure 7). When treated with **19c** at concentrations of 0, 0.05, 0.10, and 0.20 μM for 48 h, the number of K562 cells with collapsed MMP increased from 0.63% to 18.69%, 31.52% and 62.27%, respectively, suggesting that **19c** caused mitochondrial depolarization of K562 cells in the process of apoptosis.

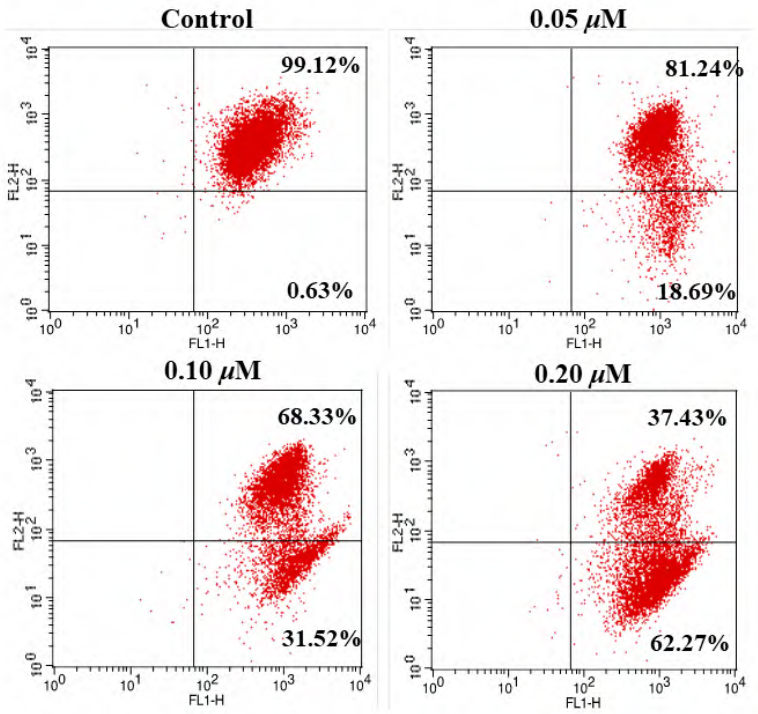

Figure 7. Effect of **19c** on the mitochondrial membrane potential of K562 cells. Incubation with different concentrations (0, 0.05, 0.10, and 0.20 μM) of **19c** in K562 cells for 48 h prior to staining with JC-1 dye, the number of cells with collapsed mitochondrial membrane potentials was determined by flow cytometry analysis.

2.8 In vitro evaluation of anti-vascular activity

To evaluate the anti-vascular activity of compound **19c**, the HUVEC culture assay was used to assess the ability to inhibit HUVEC migration, which is the key step to generate new blood vessels. As shown in Figure 8A, the untreated cells migrated to fill the area that was initially scraped after 24 h. In contrast, compound **19c** significantly inhibited the HUVEC migration in a dose-dependent manner. Then we further evaluated the anti-vascular ability of compound **19c** in a tube formation assay. After being seeded on matrigel, HUVECs form the capillary-like tubules with multicentric junctions. After exposure to **19c** at doses of 0.05, 0.10, and 0.20 μM for 6 h, the capillary-like tubes were interrupted in different levels (Figure 8B), indicating that **19c** effectively inhibited the tube formation of HUVECs. All these results demonstrated that **19c** was a potent vascular disrupting agent.

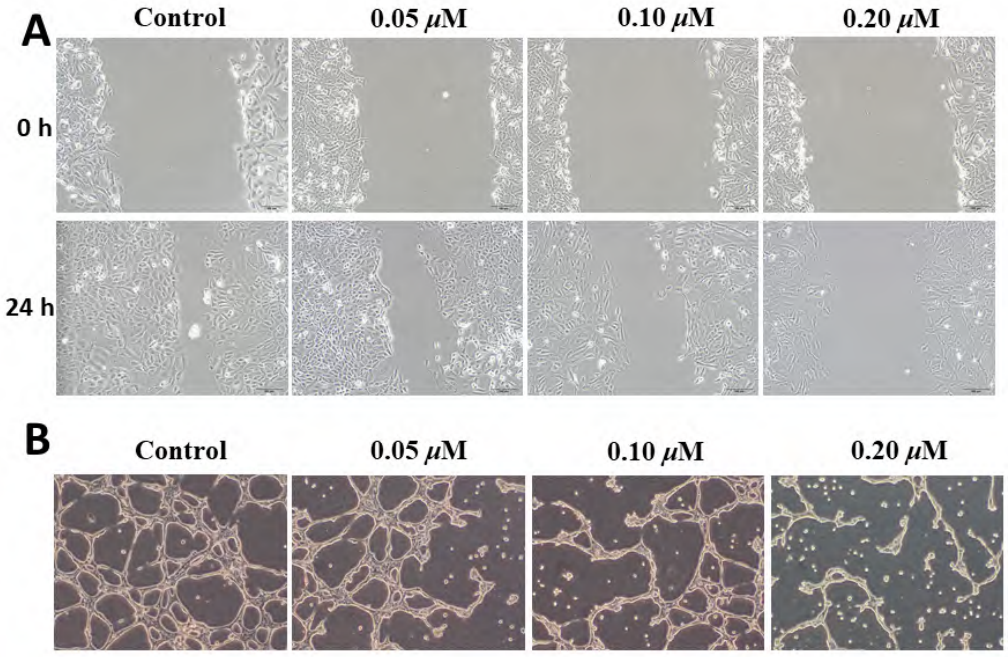

Figure 8. Effects of **19c** on the HUVECs migration and tube formation. (A) Scratches were created with sterile 200 μL pipette and images were captured using phase contrast microscopy at 0 h and 24 h after treatment with 0, 0.05, 0.1, and 0.2 μM of **19c**. (B) Images depicting the formation of HUVEC capillary-like tubular network by treatment with 0, 0.05, 0.1, and 0.2 μM of **19c** for 6h.

2.9 In vivo anti-tumor activity

To evaluate the *in vivo* anti-tumor efficacy of **19c**, human liver cancer xenograft was established by subcutaneous inoculation of H22 cells into the right flank of mice. The tumor size and the body weights of mice were monitored and recorded every 2 days. Paclitaxel (PTX) was selected as the positive control. As shown in Figure 9A, the reduction in tumor weight reached 86.6% at a dose of 8 mg/kg/2 day (i.v.) of PTX at 21 days after initiation of treatment as compared to vehicle. Compared with the vehicle group, administration of **19c** at 15 and 30 mg/kg by i.v. resulted in 50.9% and 62.6% reduction of tumor growth, respectively (Figure 9A). Notably, no significant differences in body weight or other adverse effects were observed upon treatment with **19c**, while treatment with PTX led to a significant decrease of body weight (Figure 9B). Thus, **19c** was efficacious and safe in inhibiting tumor growth with a dose-dependent manner *in vivo* and deserved further evaluation.

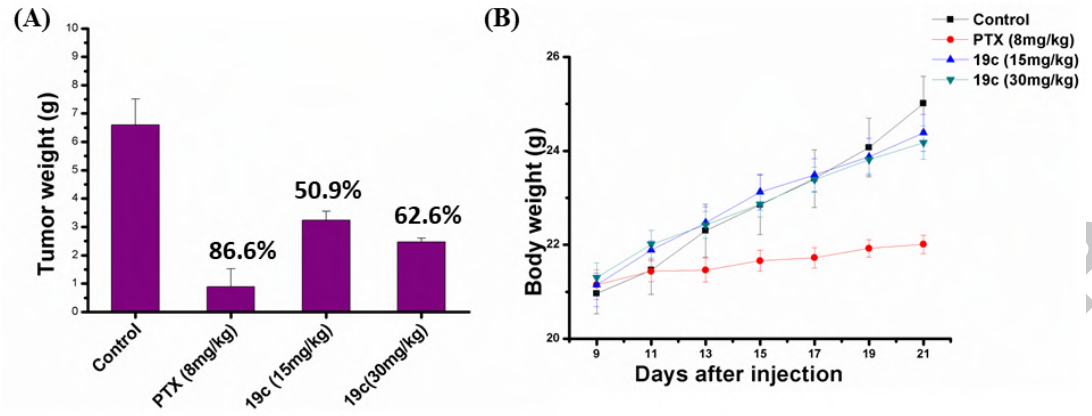

Figure 9. A) **19c** treatment resulted in significantly lower tumor weight compared with controls. B) Body weight changes of mice during treatment.

3 Conclusions

In summary, a series of novel quinazolines occupying three zones of colchicine domain have been designed, synthesized inspired by the crystal structure of verubulin analogue **6** and tubulin. Anti-proliferative screening of these newly synthesized compounds validated the representative compound **19c** as a high cytotoxic compound with IC_{50} values ranging from 0.10 to 0.13 μM against a panel of cancer cell lines, which was about 50 folds more potent than ABT-751. **19c** also displayed comparable inhibitory activity in tubulin assembly assays to ABT-751 with the IC_{50} value of 2.45 μM. The proposed binding mode of **19c** with tubulin was confirmed by molecular modeling studies which showed that it adopted a similar positioning of ABT-751 to occupy three zones of colchicine domain. Further mechanism studies demonstrated that **19c** caused cell cycle arrest in G2/M phase, induced cell apoptosis and depolarized mitochondria of K562 cells. Moreover, **19c** effectively and dose-dependently disrupted microtubule networks of K562 cells in immunofluorescent assays. The wound healing and tube formation assays also identified **19c** as a potent vascular disrupting agent. Finally, the *in vivo* anti-tumor activity of **19c** was validated in H22 liver cancer xenograft mouse model. Altogether, **19c** may represent a novel class of anti-tubulin agent with a unique binding mode with tubulin and deserves further investigation.

4 Experimental

4.1 Chemistry

4.1.1.General

Most chemicals and solvents were purchased from commercial sources. Further purification and drying by standard methods were employed when necessary. ^{1}H NMR and ^{13}C NMR spectra were recorded on Bruker-300 spectrometers in the indicated

solvents (TMS as internal standard). Data are reported as follows: chemical shift in ppm (d), multiplicity (s =singlet, d =doublet, t =triplet, q =quartet, brs = broad singlet, m =multiplet), coupling constant (Hz), and integration. High Resolution Mass measurement was performed on Agilent QTOF 6520 mass spectrometer with electron spray ionization (ESI) as the ion source. Purity of all tested compounds was ≥ 95%, as estimated by HPLC analysis. Flash column chromatography was carried out using commercially available silica gel (200-300 mesh) under pressure.

*4.1.2. Synthesis of intermediate **12.***

Intermediate **10** was synthesized according the procedures reported in the previous literature [26]. To a solution of **10 (**3.62 g, 0.015 mol) and *N*-methyl-4-methoxyaniline (2.31g, 0.017 mol) in 25 mL of anhydrous isopropanol (IPA) was added 0.6 mL of concentrated HCl, and the mixture was stirred at room temperature overnight. The mixture was extracted with CH_2Cl_2 (3 × 50 mL). The combined organic layers were then washed with brine, dried over anhydrous Na_2SO_4, and concentrated in vacuo to afford crude product **11** (4.2 g, 81.6%) as yellow solid. To a solution of **11** (4.2 g, 0.012 mol) in 20 mL CH_3OH was added 20 mL 10% NaOH aqueous, and the mixture was stirred at 80 °C for 2 h. The CH_3OH was then removed in vacuo and acidized with 10% HCl aqueous to pH 3. The yellow precipitates were collected by filtration, washed with water and dried to afford intermediate **12** (2.9 g, 76.3%) as yellow solid. ^{1}H NMR (300MHz, DMSO-d_6) δ7.91 - 7.83 (m, 1H), 7.70 (t, *J* = 7.6 Hz, 1H), 7.26 (d, *J* = 8.4 Hz, 2H), 7.20 (d, *J* = 7.6 Hz, 1H), 7.01 (d, *J* = 8.3 Hz, 2H), 6.96 (d, *J* = 8.2 Hz, 1H), 3.78 (d, J = 3.2 Hz, 3H), 3.57 (s, 3H);^{13}C NMR (75 MHz, DMSO-d_6) δ 165.98, 161.84, 158.47, 153.54, 150.87, 140.55, 133.14, 128.80, 127.82, 126.75, 126.25, 115.84, 114.16, 55.85,43.07; ESI-MS *m/z* 309.1 $[M+Na]^+$ 332.1.

*4.1.3. General procedures of compounds **13a-d**.*

To a solution of **12 (**70 mg, 0.24 mmol**)** in 5 mL CH_3CN was added 3-tetramethyluronium hexafluorophosphate (HATU) (94 mg, 0.27 mmol), Et_3N (63 μL, 0.48 mmol), various anilines (0.28 mmol) were added. The mixture was stirred for 1 h, and extracted with CH_2Cl_2 (3 × 25 mL). The combined organic layers were then washed with brine, dried over anhydrous Na_2SO_4, and concentrated in vacuo. The residue was purified by flash column chromatography to afford the products **13a-c** in 65-84% yields.

*4.1.3.1 Compound **13a.*** White solid, yield 65.1%. ^{1}H NMR (300 MHz, DMSO-d_6) δ 11.27 (s, 1H), 8.87 (s, 1H), 8.67 (d, *J* = 5.9 Hz, 2H), 8.18 (d, *J* = 5.8 Hz, 2H), 7.95 (d, *J* = 8.3 Hz, 1H), 7.76 (t, *J* = 7.6 Hz, 1H), 7.29 (d, *J* = 8.2 Hz, 2H), 7.24 (s, 1H), 7.06 - 7.02 (m, 2H), 3.82 (s, 3H), 3.68 (s, 3H); ^{13}C NMR (75 MHz, DMSO) δ 163.21, 161.39, 158.12, 152.73, 150.62, 148.42, 146.85, 139.95, 132.76, 128.74, 127.33, 126.57,

125.90, 115.76, 115.39, 114.56, 55.37, 45.82; HR-MS (ESI) m/z: calcd for $C_{22}H_{20}N_5O_2$ $[M+H]^+$ 386.1612, found 386.1606.

4.1.3.2 Compound ***13c.*** White solid, yield 72.0%. ^{1}H NMR (300 MHz, $CDCl_3$) δ 10.08 (s, 1H), 8.05 - 7.95 (m, 1H), 7.75 (d, *J* = 9.0 Hz, 2H), 7.64 - 7.59 (m, 1H), 7.15 (d, *J* = 8.9 Hz, 2H), 7.11 - 7.06 (m, 1H), 7.06 - 7.03 (m, 1H), 6.95 (d, *J* = 2.5 Hz, 2H), 6.92 (d, *J* = 2.6 Hz, 2H), 3.85 (s, 3H), 3.81 (s, 3H), 3.72 (s, 3H); ^{13}C NMR (75 MHz, $CDCl_3$) δ 161.28, 160.46, 158.01, 155.88, 152.37, 151.02, 140.08, 131.82, 130.74, 128.94, 126.93, 125.76, 125.66, 120.70, 115.77, 114.92, 113.75, 55.04, 54.99, 42.48; HR-MS (ESI) m/z: calcd for $C_{24}H_{23}N_4O_3$ [M+H]+ 415.1765, found 415.1762.

4.1.3.3 Compound ***13d.*** **13b** was obtained as colorless oil which was used for next step directly. To a solution of **13b** (50 mg, 0.10 mmol) in THF was added TBAF (30 mg, 0.12 mmol), and the reaction was stirred at room temperature for 30 min. Then, the mixture was extracted with CH_2Cl_2 (3 × 25 mL). The combined organic layers were washed with brine, dried over anhydrous Na_2SO_4, and concentrated in vacuo. The residue was purified by flash column chromatography to afford the product **13d** as white solid in 62.3% yield over two steps. ^{1}H NMR (300 MHz, DMSO-d_6) δ 10.34 (s, 1H), 9.33 (s, 1H), 7.90 (d, *J* = 8.3 Hz, 1H), 7.73 (d, *J* = 7.5 Hz, 1H), 7.67 (d, *J* = 8.8 Hz, 2H), 7.29 (d, *J* = 7.9 Hz, 2H), 7.21 (t, *J* = 7.8 Hz, 1H), 7.04 (s, 1H), 7.02 (d, *J* = 7.9 Hz, 2H), 6.81 (d, *J* = 8.8 Hz, 2H), 3.80 (s, 3H), 3.65 (s, 3H); ^{13}C NMR (75 MHz, DMSO) δ 161.31, 161.23, 157.96, 153.91, 153.88, 150.99, 140.26, 132.53, 130.06, 128.77, 127.34, 126.03, 125.80, 121.76, 115.59, 115.36, 115.13, 55.37, 42.67; HR-MS (ESI) m/z: calcd for $C_{23}H_{21}N_4O_3$ $[M+H]^+$ 401.1608, found 401.1613.

4.1.4. Synthesis of intermediate ***18.***

Intermediate **17** was synthesized according the procedures reported in the previous literature [27]. To a solution of **17** (3.2 g, 0.016 mol) in 50 mL THF was added Et_3N (3.3 mL, 0.024 mol) and *N*-methyl-4-methoxyaniline (1.9 g, 0.014 mol), and the mixture was stirred at room temperature overnight. The mixture was extracted with CH_2Cl_2 (3 × 50 mL). The combined organic layers were then washed with brine, dried over anhydrous Na_2SO_4, and concentrated in vacuo. The residue was then purified by flash column chromatography using PE/EA 15:1 as the fluent to afford **18** (3.9 g, 81.3%) as white powder. 1H NMR (300 MHz, $CDCl_3$) δ 7.64 (d, *J* = 8.4 Hz, 1H), 7.47 (t, *J* = 7.8 Hz, 1H), 7.07 (d, *J* = 8.8 Hz, 2H), 6.89 (m, 4H), 3.78 (s, 3H), 3.52 (s, 3H); ^{13}C NMR (75 MHz, $CDCl_3$) δ 162.54, 158.68, 156.56, 152.98, 139.94, 132.57, 127.65, 127.49, 126.38, 124.93, 115.44, 114.78, 55.56, 43.26; ESI-MS *m/z* 299.1 $[M+H]^+$ 300.1.

4.1.5. General procedures of compounds ***19a-t.***

To a solution of **18** (75 mg, 0.25 mmol) in 5 mL EtOH in sealed tube was added various anilines or benzylamines, the mixture was stirred at 150 °C. After completion, the reaction was cooled to room temperature. In the cases of solid precipitation in the

reaction, the precipitates were collected by filtration, washed with cold EtOH and dried to afford the final products. When no solid precipitated in the reaction, the solvent was removed in vacuo and then purified by flash column chromatography to afford the final products.

*4.1.5.1. Compound **19a***. White solid, yield 76.7%. ^{1}H NMR (300 MHz, DMSO-d_6) δ 9.36 (s, 1H), 9.33 (s, 1H), 9.31 (s, 1H), 7.77 - 7.67 (m, 2H), 7.35 (d, *J* = 8.9 Hz, 2H), 7.16 (d, *J* = 7.8 Hz, 2H), 7.14 - 7.10 (m, 1H), 6.86 (d, *J* = 8.5 Hz, 1H), 3.83 (s, 3H), 3.65 (s, 3H); ^{13}C NMR (75 MHz, DMSO-d_6) δ 161.83, 160.96, 158.52, 151.11, 150.14, 139.04, 137.76, 129.81, 127.73, 127.61, 126.15, 125.29, 115.52, 114.53, 109.23, 55.49, 43.25; HR-MS (ESI) m/z: calcd for $C_{21}H_{20}N_5O$ $[M+H]^+$ 358.1662, found 358.1659.

*4.1.5.2. Compound **19b***. White solid, yield 66.9%. ^{1}H NMR (300 MHz, $CDCl_3$) δ 8.56 (d, *J* = 5.1 Hz, 2H), 7.57 (d, *J* = 8.3 Hz, 1H), 7.49 (t, *J* = 7.7 Hz, 1H), 7.36 (d, *J* = 5.1 Hz, 2H), 7.13 (d, *J* = 8.6 Hz, 2H), 6.97 (d, *J* = 8.7 Hz, 2H), 6.87 - 6.76 (m, 1H), 6.67 (d, *J* = 8.6 Hz, 1H), 4.88 (s, 1H), 4.77 (s, 2H), 3.87 (s, 3H), 3.45 (s, 3H); ^{13}C NMR (75 MHz, $CDCl_3$) δ161.35, 159.42, 149.84, 147.90, 144.14, 138.26, 134.12, 134.10, 127.46, 127.22, 122.90, 122.06, 119.25, 115.70, 110.46, 77.48, 77.06, 76.64, 55.63, 44.13, 43.84; HR-MS (ESI) m/z: calcd for $C_{22}H_{22}N_5O_2$ $[M+H]^+$ 372.1819, found 372.1815.

*4.1.5.3. Compound **19c***. White solid, yield 79.2%. ^{1}H NMR (300 MHz, $CDCl_3$) δ 8.58 (s, 1H), 8.46 - 8.30 (m, 1H), 7.72 (d, *J* = 7.9 Hz, 1H), 7.42 (d, *J* = 8.4 Hz, 1H), 7.36 – 7.30 (m, 1H), 7.24 - 7.15 (m, 1H), 7.04 (d, *J* = 8.9 Hz, 2H), 6.86 (d, *J* = 8.8 Hz, 2H), 6.65 (d, *J* = 6.9 Hz, 2H), 6.21 (s, 1H), 4.68 (s, 2H), 3.76 (s, 3H), 3.42 (s, 3H); ^{13}C NMR (75 MHz, $CDCl_3$) δ 179.38, 161.20, 158.41, 148.44, 147.96, 138.70, 138.68, 138.64, 134.82, 134.20, 132.87, 126.92, 126.53, 123.09, 121.51, 114.98, 110.50, 55.06, 43.07, 42.23; HR-MS (ESI) m/z: calcd for $C_{22}H_{22}N_5O$ $[M+H]^+$ 372.1819, found 372.1816.

*4.1.5.4. Compound 19**d***. White solid, yield 75.2%. ^{1}H NMR (300 MHz, $CDCl_3$) δ 8.21 (s, 1H), 7.68 (dd, *J* = 8.4, 2.5 Hz, 1H), 7.45 (d, *J* = 8.3 Hz, 1H), 7.40 - 7.34 (m, 1H), 7.10 (d, *J* = 8.6 Hz, 2H), 6.94 - 6.87 (m, 2H), 6.83 (d, *J* = 8.4 Hz, 1H), 6.69 (m, 2H), 6.10 (s, 1H), 4.67 (s, 2H), 3.92 (s, 3H), 3.82 (s, 3H), 3.48 (s, 3H); ^{13}C NMR (75 MHz, $CDCl_3$) δ 162.99, 161.95, 157.60, 157.31, 151.59, 145.48, 140.46, 138.17, 131.73, 127.62, 126.87, 126.25, 123.87, 120.21, 114.67, 111.76, 110.25, 55.00, 52.91, 42.48, 42.01; HR-MS (ESI) m/z: calcd for $C_{23}H_{24}N_5O_2$ $[M+H]^+$ 402.1925, found 402.1918.

*4.1.5.5. Compound **19f***. To a solution of **19e** (50 mg, 0.10 mmol) in THF was added TBAF (32 mg, 0.12 mmol), and the reaction was stirred at room temperature for 30 min. Then, the mixture was extracted with CH_2Cl_2 (3 × 25 mL). The combined organic layers were washed with brine, dried over anhydrous Na_2SO_4, and concentrated in vacuo. The residue was purified by flash column chromatography to afford the product **19f** as white solid in 46.8% yield over two steps. ^{1}H NMR (300 MHz, DMSO-d_6) δ 10.27 (s, 1H), 9.57 (s, 1H), 7.63 (t, *J* = 7.8 Hz, 1H), 7.53 (d, *J* = 8.3 Hz, 1H), 7.42 (d, *J* = 4.9 Hz, 2H), 7.39 (d, *J* = 4.9 Hz, 2H), 7.09 (d, *J* = 8.4 Hz, 2H), 6.97 (t, *J* = 7.9 Hz,

1H), 6.86 (d, *J* = 8.3 Hz, 2H), 6.72 (d, *J* = 8.5 Hz, 1H), 3.83 (s, 3H), 3.57 (s, 3H); ^{13}C NMR (75 MHz, DMSO) δ 160.94, 158.90, 154.94, 138.08, 138.06, 134.25, 128.11, 127.64, 126.97, 124.07, 123.03, 118.43, 118.32, 115.54, 115.47, 110.66, 55.51, 43.67; HR-MS (ESI) m/z: calcd for $C_{22}H_{21}N_4O_2$ $[M+H]^+$ 373.1659, found 373.1659.

4.1.5.6. Compound ***19g***. White solid, yield 86.5%. ^{1}H NMR (300 MHz, $CDCl_3$) δ 10.48 (s, 1H), 7.56 (d, *J* = 8.8 Hz, 2H), 7.48 (t, *J* = 7.6 Hz, 1H), 7.31 (s, 1H), 7.20 (d, *J* = 8.4 Hz, 2H), 7.01 (d, *J* = 8.4 Hz, 2H), 6.87 (d, *J* = 8.8 Hz, 2H), 6.82 (s, 1H), 6.67 (d, *J* = 8.6 Hz, 1H), 3.88 (s, 3H), 3.80 (s, 3H), 3.62 (s, 3H); ^{13}C NMR (75 MHz, $CDCl_3$) δ 160.74, 159.22, 156.44, 150.40, 140.73, 137.21, 133.96, 129.21, 127.00, 126.85, 123.16, 122.90, 117.78, 115.35, 113.46, 109.75, 55.17, 54.95, 43.96; HR-MS (ESI) m/z: calcd for $C_{23}H_{23}N_4O_2$ $[M+H]^+$ 387.1816, found 387.1814.

4.1.5.7. Compound ***19h***. White solid, yield 73.2%. ^{1}H NMR (300 MHz, $CDCl_3$) δ 7.44 (d, *J* = 8.4 Hz, 1H), 7.37 (s, 1H), 7.34 (d, *J* = 7.8 Hz, 2H), 7.08 (d, *J* = 8.4 Hz, 2H), 6.88 - 6.85 (m, 5H), 6.66 (t, *J* = 7.7 Hz, 1H), 5.47 (s, 1H), 4.70 (s, 2H), 3.81 (s, 3H), 3.78 (s, 3H), 3.46 (s, 3H); ^{13}C NMR (75 MHz, $CDCl_3$) δ 162.17, 158.26, 158.21, 157.30, 153.34, 141.10, 131.66, 131.33, 128.47, 126.82, 126.18, 124.96, 119.66, 114.56, 113.38, 112.17, 54.98, 54.78, 44.66, 42.25; HR-MS (ESI) m/z: calcd for $C_{24}H_{25}N_4O_2$[M+H]+401.1972, found 401.1968.

4.1.5.8. Compound ***19i***. White solid, yield 75.3%. ^{1}H NMR (300 MHz, $CDCl_3$) 8.64 (s, 1H), 7.54 (d, J = 8.3 Hz, 1H), 7.47 (t, J = 7.6 Hz, 1H), 7.39 (dd, J = 8.4, 5.3 Hz, 2H), 7.19 - 7.12 (m, 2H), 7.06 - 6.97 (m, 4H), 6.81 (t, J = 7.9 Hz, 1H), 6.67 (d, J = 8.5 Hz, 1H), 4.73 (s, 2H), 3.87 (s, 3H), 3.57 (s, 3H); ^{13}C NMR (75 MHz, $CDCl_3$) δ 163.18, 160.76, 159.93, 158.93, 153.07, 133.59, 133.29, 128.56, 128.46, 126.96, 126.77, 122.41, 115.21, 115.06, 114.77, 109.82, 55.14, 43.90, 43.49; HR-MS (ESI) m/z: calcd for $C_{23}H_{22}FN_4O$ $[M+H]^+$ 389.1772, found 389.1768 .

4.1.5.9. Compound ***19j***. White solid, yield 83.3%. ^{1}H NMR (300 MHz, $CDCl_3$) δ 7.65 (s, 1H), 7.46 (dd, *J* = 8.3, 1.4 Hz, 1H), 7.41 (d, *J* = 1.3 Hz, 1H), 7.37 (d, *J* = 8.4 Hz, 2H), 7.10 (d, *J* = 7.7 Hz, 2H), 7.07 (d, *J* = 7.0 Hz, 2H), 6.90 (d, *J* = 8.9 Hz, 2H), 6.75 - 6.69 (m, 1H), 6.59 (d, *J* = 8.6 Hz, 1H), 4.69 (s, 2H), 3.79 (s, 3H), 3.46 (s, 3H); ^{13}C NMR (75 MHz, $CDCl_3$) δ 160.81, 158.90, 153.28, 147.85, 137.74, 136.58, 133.54, 128.20, 126.96, 126.92, 126.74, 122.32, 121.61, 120.59, 120.51, 118.18, 115.19, 109.89, 55.11, 43.83, 43.40; HR-MS (ESI) m/z: calcd for $C_{24}H_{22}F_3N_4O_2$ $[M+H]^+$ 455.1689, found 455.1687.

4.1.5.10. Compound ***19k***. White solid, yield 82.1%. ^{1}H NMR (300 MHz, $CDCl_3$) δ 8.76 (s, 1H), 7.50 (d, *J* = 8.3 Hz, 1H), 7.37 (t, *J* = 7.6 Hz, 1H), 7.26 (d, *J* = 8.2 Hz, 2H), 7.08 (d, *J* = 8.3 Hz, 2H), 6.91 (d, *J* = 8.4 Hz, 2H), 6.77 (d, *J* = 8.3 Hz, 2H), 6.70 (d, *J* = 7.3 Hz, 1H), 6.53 (d, *J* = 8.6 Hz, 1H), 4.61 (s, 2H), 3.92 (q, *J* = 6.9 Hz, 2H), 3.79 (s, 3H), 3.52 (s, 3H), 1.31 (t, *J* = 6.9 Hz, 3H); ^{13}C NMR (75 MHz, $CDCl_3$) δ 160.57, 159.10, 157.77, 152.09, 140.61, 137.35, 133.81, 129.19, 128.25, 127.04, 126.77, 122.62,

117.58, 115.27, 114.04, 109.48, 62.93, 55.17, 44.07, 43.70, 29.18; HR-MS (ESI) m/z: calcd for $C_{25}H_{27}N_4O_2[M+H]^+$ 415.2129, found 415.2120.

4.1.5.11. Compound ***19l****.* White solid, yield 76.5%. ^{1}H NMR (300 MHz, $CDCl_3$) δ 7.45 (d, *J* = 8.5 Hz, 1H), 7.37 (d, *J* = 6.9 Hz, 1H), 7.35 - 7.30 (m, 2H), 7.09 (d, *J* = 8.4 Hz, 2H), 6.89 (s, 1H), 6.89 - 6.86 (m, 2H), 6.83 (s, 2H), 6.66 (t, *J* = 7.7 Hz, 1H), 5.45 (s, 1H), 4.68 (s, 2H), 4.58 - 4.48 (m, 1H), 3.81 (s, 3H), 3.46 (s, 3H), 1.32 (d, *J* = 6.1 Hz, 6H); ^{13}C NMR (75 MHz, $CDCl_3$) δ 162.14, 158.14, 157.33, 156.51, 153.07, 141.02, 131.39, 128.49, 126.83, 126.20, 124.81, 124.81, 119.72, 115.43, 114.57, 112.11, 69.43, 54.99, 44.67, 42.29, 21.59; HR-MS (ESI) m/z: calcd for $C_{26}H_{29}N_4O_2$ $[M+H]^+$ 429.2285, found 429.2275.

4.1.5.12. Compound ***19m.*** White solid, yield 78.9%. ^{1}H NMR (300 MHz, $CDCl_3$) δ 9.19 (s, 1H), 7.64 (d, *J* = 8.0 Hz, 2H), 7.57 - 7.49 (m, 4H), 7.17 (d, *J* = 8.7 Hz, 2H), 7.01 (d, *J* = 8.3 Hz, 2H), 6.86 (t, *J* = 7.1 Hz, 1H), 6.65 (d, *J* = 8.6 Hz, 1H), 4.84 (d, *J* = 5.9 Hz, 2H), 3.89 (s, 3H), 3.53 (s, 3H); ^{13}C NMR (75 MHz, $CDCl_3$) δ 160.51, 159.28, 152.35, 142.84, 142.79, 140.24, 136.95, 134.13, 131.94, 127.29, 126.93, 123.10, 118.15, 117.51, 115.36, 110.71, 109.53, 55.18, 44.13, 43.70; HR-MS (ESI) m/z: calcd for $C_{24}H_{22}N_5O$ $[M+H]^+$ 396.1819, found 396.1814.

4.1.5.13. Compound ***19n****.* White solid, yield 88.1%. ^{1}H NMR (300 MHz, $CDCl_3$) δ 7.46 (s, 1H), 7.35 (t, *J* = 7.6 Hz, 1H), 7.16 (t, *J* = 7.9 Hz, 1H), 7.05 (d, *J* = 8.4 Hz, 2H), 6.93 (d, *J* = 6.8 Hz, 2H), 6.88 (d, *J* = 8.7 Hz, 2H), 6.74 - 6.60 (m, 3H), 5.87 (s, 1H), 4.66 (s, 2H), 3.77 (s, 3H), 3.72 (s, 3H), 3.45 (s, 3H); ^{13}C NMR (75 MHz, $CDCl_3$) δ 161.05, 159.32, 158.56, 158.55, 139.64, 139.62, 138.43, 138.41, 133.06, 129.04, 126.97, 126.97, 126.59, 121.75, 119.22, 115.04, 112.42, 112.34, 55.10, 54.81, 44.75, 43.23; HR-MS (ESI) m/z: calcd for $C_{24}H_{25}N_4O_2$ $[M+H]^+$ 401.1972, found 401.1969.

4.1.5.14. Compound ***19o****.* White solid, yield 79.2%. ^{1}H NMR (300 MHz, $CDCl_3$) δ 7.44 (d, *J* = 8.4 Hz, 1H), 7.39 - 7.33 (m, 1H), 7.09 (d, *J* = 8.8 Hz, 2H), 7.01 - 6.94 (m, 2H), 6.92 – 6.84 (m, 3H), 6.82 (d, *J* = 8.1 Hz, 1H), 6.69 - 6.64 (m, 1H), 5.50 (s, 1H), 4.69 (s, 2H), 3.86 (s, 3H), 3.85 (s, 3H), 3.81 (s, 3H), 3.47 (s, 3H); ^{13}C NMR (75 MHz, $CDCl_3$) δ 162.17, 158.27, 157.32, 153.32, 148.49, 147.59, 141.04, 132.13, 131.36, 126.81, 126.19, 124.93, 119.70, 119.39, 114.56, 112.15, 110.65, 110.61, 55.44, 55.36, 54.98, 45.09, 42.26; HR-MS (ESI) m/z: calcd for $C_{25}H_{27}N_4O_3$ $[M+H]^+$ 431.2078, found 431.2074.

4.1.5.15. Compound ***19p****.* White solid, yield 68.3%. ^{1}H NMR (300 MHz, $CDCl_3$) δ 8.96 (s, 1H), 7.58 - 7.46 (m, 2H), 7.19 (d, *J* = 8.8 Hz, 2H), 7.01 (d, *J* = 8.9 Hz, 2H), 6.88 - 6.82 (m, 1H), 6.69 (s, 2H), 6.65 (d, *J* = 8.8 Hz, 1H), 4.72 (s, 2H), 3.89 (s, 9H), 3.83 (s, 3H), 3.64 (s, 3H); ^{13}C NMR (75 MHz, $CDCl_3$) δ 160.57, 159.19, 152.88, 152.23, 140.36, 137.15, 136.69, 133.96, 132.66, 126.98, 126.89, 122.83, 117.43, 115.32, 109.48, 103.84, 60.31, 55.79, 55.16, 44.79, 43.69; HR-MS (ESI) m/z: calcd for $C_{26}H_{29}N_4O_4$ $[M+H]^+$ 461.2183, found 461.2181.

*4.1.5.16. Compound **19q***. White solid, yield 81.4%. ^{1}H NMR (300 MHz, $CDCl_3$) δ 7.45 (d, *J* = 8.3 Hz, 1H), 7.41 - 7.30 (m, 1H), 7.26 (s, 1H), 7.15 (d, *J* = 7.9 Hz, 1H), 7.09 (d, *J* = 8.6 Hz, 2H), 6.88 (d, *J* = 8.5 Hz, 2H), 6.84 (s, 1H), 6.79 – 6.62 (m, 2H), 5.63 (s, 1H), 4.67 (s, 2H), 4.54 (t, *J* = 8.7 Hz, 2H), 3.81 (s, 3H), 3.48 (s, 3H), 3.16 (t, *J* = 8.7 Hz, 2H); ^{13}C NMR (75 MHz, $CDCl_3$) δ 162.07, 158.78, 157.78, 157.47, 140.84, 131.50, 131.37, 127.11, 126.82, 126.75, 126.21, 124.43, 124.06, 124.06, 119.86, 114.63, 112.00, 108.50, 70.76, 54.99, 44.89, 42.33, 29.24; HR-MS (ESI) m/z: calcd for $C_{25}H_{25}N_4O_2$ $[M+H]^+$ 413.1972, found 413.1966.

*4.1.5.17. Compound **19r***. White solid, yield 76.3%. ^{1}H NMR (300 MHz, $CDCl_3$) δ 8.24 (s, 1H), 7.48 - 7.42 (m, 1H), 7.26 (d, *J* = 8.0 Hz, 2H), 7.14 (d, *J* = 8.4 Hz, 2H), 6.95 (d, *J* = 8.4 Hz, 2H), 6.87 (d, *J* = 8.2 Hz, 2H), 6.76 (d, *J* = 4.0 Hz, 2H), 5.01 (s, 2H), 3.85 (s, 3H), 3.79 (s, 3H), 3.54 (s, 3H), 3.42 (s, 3H).^{13}C NMR (75 MHz, $CDCl_3$) δ 160.69, 158.52, 158.27, 141.56, 139.08, 132.73, 128.75, 128.37, 126.95, 126.10, 121.73, 121.62, 121.49, 114.92, 113.56, 110.25, 57.71, 55.08, 54.79, 52.31, 43.02; HR-MS (ESI) m/z: calcd for $C_{25}H_{27}N_4O_2$ $[M+H]^+$ 415.2129, found 415.2126.

*4.1.5.18. Compound **19s***. White solid, yield 81.2%. ^{1}H NMR (300 MHz, $CDCl_3$) δ 8.95 (s, 1H), 7.51 (d, *J* = 8.3 Hz, 1H), 7.46 (d, *J* = 7.1 Hz, 1H), 7.39 (d, *J* = 8.3 Hz, 2H), 7.14 (d, *J* = 8.7 Hz, 2H), 6.99 (d, *J* = 8.9 Hz, 2H), 6.88 (d, *J* = 8.5 Hz, 2H), 6.83 – 6.74 (m, 1H), 6.59 (d, *J* = 8.6 Hz, 1H), 5.29 - 5.11 (m, 1H), 3.88 (s, 3H), 3.78 (s, 3H), 3.54 (s, 3H), 1.66 (d, *J* = 6.9 Hz, 3H); ^{13}C NMR (75 MHz, $CDCl_3$) δ 160.37, 159.10, 158.21, 151.36, 140.40, 137.25, 135.31, 133.77, 127.00, 126.80, 126.61, 122.59, 117.37, 115.26, 113.47, 109.36, 55.15, 54.76, 50.89, 43.66, 22.89; HR-MS (ESI) m/z: calcd for $C_{25}H_{27}N_4O_2$ $[M+H]^+$ 415.2129, found 415.2122.

*4.1.5.19. Compound **19t***. White solid, yield 80.1%. ^{1}H NMR (300 MHz, $CDCl_3$) δ 7.52 (d, *J* = 8.4 Hz, 1H), 7.37 - 7.32 (m, 1H), 7.16 (d, *J* = 8.3 Hz, 1H), 7.09 (d, *J* = 8.4 Hz, 2H), 6.98 - 6.89 (m, 1H), 6.87 (d, *J* = 7.9 Hz, 2H), 6.77 (d, *J* = 8.3 Hz, 1H), 6.71 (s, 1H), 6.68 - 6.56 (m, 1H), 5.01 (s, 2H), 4.19 (t, *J* = 5.9 Hz, 2H), 3.80 (s, 3H), 3.79 (s, 3H), 3.54 (s, 3H), 2.96 (t, *J* = 5.9 Hz, 2H); ^{13}C NMR (75 MHz, $CDCl_3$) δ 161.75, 157.57, 157.46, 157.30, 153.47, 141.24, 136.16, 131.23, 127.02, 126.85, 126.58, 126.07, 125.19, 119.53, 114.56, 112.89, 111.82, 111.44, 54.98, 54.81, 45.51, 42.30, 41.10, 29.03; HR-MS (ESI) m/z: calcd for $C_{26}H_{27}N_4O_2$ $[M+H]^+$ 427.2129, found 427.2199.

4.2. Pharmacology

4.2.1. In vitro anti-proliferative assay

K562, HepG2, KB, HCT-8 and MDB-MD-231 cells were purchased from Nanjing KeyGen Biotech Co. Ltd. (Nanjing, China). The cytotoxicity of the test compounds was determined using the MTT assay. Briefly, the cell lines were incubated at 37 °C in a humidified 5% CO_2 incubator for 24 h in 96-microwell plates. After medium removal, 100 mL of culture medium with 0.1% DMSO containing the test compounds at different

concentrations was added to each well and incubated at 37 °C for another 72 h. The MTT (5 mg/mL in PBS) was added and incubated for another 4 h, the optical density was detected with a microplate reader at 490 nm. The IC_{50} values were calculated according to the dose-dependent curves. All the experiments were repeated in at least three independent experiments.

4.2.2. In vitro tubulin polymerization inhibitory assay

An amount of 2 mg/mL tubulin (Cytoskeleton) was resuspended in PEM buffer containing 80 mM piperazine-N,N'-bis(2-ethanesulfonic acid) sequisodium salt PIPES (pH 6.9), 0.5 mM EGTA, 2 mM $MgCl_2$, and 15% glycerol. Then the mixture was preincubated with compounds or vehicle DMSO on ice. PEG containing GTP was added to the final concentration of 3 mg/mL before detecting the tubulin polymerization reaction. After 30 min, the absorbance of different concentrations was detected by a spectrophotometer at 340 nm at 37 °C. The area under the curve was used to determine the concentration that inhibited tubulin polymerization by 50% (IC_{50}), which was calculated with GraphPad Prism Software version 5.02.

4.2.3. Molecular modeling study

The X-ray structure of the ABT-751-*α,β*-tubulin complex was downloaded from the Protein Data Bank (PDB code: 3HKC). The protein was prepared by removal of the stathmin-like domain, subunits C and D, water molecules and ABT-751 using Discovery Studio modules. The docking procedure was performed by employing DOCK program in Discovery Studio 3.0 software, and the structural image was obtained using PyMOL software.

4.2.4. Immunofluorescence staining

K562 cells were seeded into 6-well plates and then treated with vehicle control 0.1% DMSO, **19c** (0.05 μM, 0.1 μM, 0.2 μM) for 24 h. The cells were fixed with 4% paraformaldehyde and then penetrated with PBS for three times. After blocking for 20 min by adding 50-100 μL goat serum albumin at room temperature, cells were incubated with a monoclonal antibody (anti-*α*-tubulin) at 37 °C for 2 h. Then the cells were washed three times by PBS following staining by fluorescence antibody and labeling of nuclei by 4,6-diamidino-2-phenylindole (DAPI). Cells were finally visualized using a fluorescence microscope (OLYMPUS, Japan).

4.2.5. Cell cycle analysis

K562 cells were seeded into 6-well plates and incubated at 37 °C in a humidified 5% CO_2 incubator for 24 h, and then with vehicle control 0.1% DMSO, **19c** (0.05 μM, 0.1 μM, 0.2 μM) for 48 h. The collected cells were fixed by adding 70% ethanol at 4 °C for 12 h. Subsequently, the cells were resuspended in PBS containing 100 mL RNase A and 400 mL of propidium iodide for 30 min. The DNA content of the cells was measured using a FACS Calibur flow cytometer (BectoneDickinson, San Jose, CA, USA).

4.2.6. Cell apoptosis analysis

After treatment with vehicle control 0.1% DMSO, **19c** (0.05 μM, 0.1 μM, 0.2 μM) for 48 h, the cells were washed twice in PBS, centrifuged and resuspended in 500 mL AnnexinV binding buffer. The cells were then harvested, washed and stained with 5 mL Annexin V-APC and 5 mL 7-AAD in the darkness for 15 min. Apoptosis was analyzed using a FACS Calibur flow cytometer (BectoneDickinson, San Jose, CA, USA).

4.2.7. Mitochondrial membrane potential analysis

After treatment with vehicle control 0.1% DMSO, **19c** (0.05 μM, 0.1 μM, 0.2 μM) for 48 h, the cells were washed in PBS and resuspended in 500 mL JC-1 incubation buffer at 37 °C for 15 min. Then, **19c** was immediately assessed for a red fluorescence using a microplate reader (ELx80, Bio-Tek, USA). The fluorescent signal of monomers was measured with an excitation wavelength of 488 nm. The percentage of cells with healthy or collapsed mitochondrial membrane potentials was monitored by flow cytometry analysis (Bectone-Dickinson, San Jose, CA, USA).

4.2.8. Wound healing assay

K562 cells were grown in 6-well plates for 24 h. Scratches were made in confluent monolayers using 200 μL pipette tip. Then, wounds were washed twice with PBS to remove non-adherent cell debris. The media containing different concentrations (0.05 μM, 0.1 μM, 0.2 μM) of the compound **19c** were added to the petridishes. Cells which migrated across the wound area were photographed using phase contrast microscopy at 0 h and 24 h.

4.2.9. Tube formation assay

EC Matrigel matrix was thawed at 4 °C overnight, and HUVECs suspended in DMEM were seeded in 96-well culture plates at a cell density of 50,000 cells/well after polymerization of the Matrigel at 37 °C for 30 min. They were then treated with 20 μL different concentrations (0.05 μM, 0.1 μM, 0.2 μM) of compound **19c** or vehicle for 6 h at 37 °C. Then, the morphological changes of the cells and tubes formed were observed and photographed under inverted microscope (OLYMPUS, Japan).

4.2.10. In vivo anti-tumor evaluation

Five-week-old male Institute of Cancer Research (ICR) mice were purchased from Shanghai SLAC Laboratory Animals Co. Ltd. A total of 1×10^6 H22 cells were subcutaneously inoculated into the right flank of ICR mice according to protocols of tumor transplant research, to initiate tumor growth. After incubation for one day, mice were weighted and at random divided into four groups of eight animals. The groups treated with **19c** were administered 15, 30 mg/kg in a vehicle of 10% DMF/2% Tween 80/88% saline, respectively. The positive control group was treated with PTX (8 mg/kg) every 2 days by intravenous injection. The negative control group received a vehicle of 10% DMF/2% Tween 80/88% saline through intravenous injection. Treatments of **19c**

were done at a frequency of intravenous injection one dose per day for a total 21 consecutive days while the positive group was treated with PTX one dose per two days. The mice were sacrificed after the treatments and the tumors were excised and weighed. The inhibition rate was calculated as follows: Tumor inhibitory ratio (%) = (1-average tumor weight of treated group/average tumor weight of control group) × 100%.

Acknowledgments

The authors acknowledge the National Natural Science Foundation of China (No. 81673306, 81703348), The Open Project of State Key Laboratory of Natural Medicines, China Pharmaceutical University (No. SKLNMKF 201710), Key Laboratory for the Chemistry and Molecular Engineering of Medicinal Resources (Guangxi Normal University), Ministry of Education of China (No. CMEMR2013-B05), and China Postdoctoral Science Foundation (No. 2017T100424) for financial support.

References

1. R.A. Stanton, K.M. Gernert, J.H. Nettles, R. Aneja, Med. Res. Rev. 31 (2011) 443-481.
2. J. Howard, A.A. Hyman, Dynamics and mechanics of the microtubule plus end, Nature 422 (2003), 753.
3. M. Jordan, L. Wilson, Microtubules as a target for anticancer drugs, Nat. Rev. Cancer 4 (2004) 253-265.
4. M. N. Islam, M. N Iskander, Microtubulin binding sites as target for developing anticancer agents, Mini-Rev. Med. Chem. 4 (2004), 1077-1104.
5. C. Dumontet, M. Jordan, Microtubule-binding agents: a dynamic field of cancer therapeutics, Nat. Rev. Drug Discov. 9 (2010) 790-803.
6. E. Hamel, Antimitotic natural products and their interactions with tubulin, Med. Res. Rev. 16 (1996) 207-231
7. M. J. Perez-Perez, E. M. Priego, O. Bueno, M.S. Martins, M. D. Canela, S. Liekens, Blocking Blood Flow to Solid Tumors by Destabilizing Tubulin: An Approach to Targeting Tumor Growth, J. Med. Chem. 59 (2016) 8685-8711.
8. Y. Ji, Y. Liu, Z. Liu, Tubulin colchicine binding site inhibitors as vascular disrupting agents in clinical developments, Curr. Med. Chem. 22 (2015) 1348-1360.
9. Y. Liu, H. Chen, H. Lee, J. Liou, Tubulin inhibitors: A patent review, Expert Opin. Ther. Pat. 24 (2014) 69 - 88.
10. A. Dorléans, B. Gigant, R. B. G. Ravelli, P. Mailliet, V. Mikol, M. Knossow, Variations in the colchicine-binding domain provide insight into the structural

switch of tubulin, Proc. Natl. Acad. Sci. 106 (2009) 13775-13779.

11. A. Massarotti, A. Coluccia, R. Silvestri, G. Sorba, A. Brancale, The tubulin colchicine domain: a molecular modeling perspective, ChemMedChem 7 (2012) 33-42.
12. W. Li, H. Sun, S. Sun, Z. Zhu, J. Xu, Tubulin inhibitors targeting the colchicine binding site: a perspective of privileged structures, Future med. chem. 9 (2017) 1765-1794.
13. H. Yoshino, N. Ueda, J. Niijima, H. Sugumi, Y. Kotake, N. Koyanagi, K. Yoshimatsu, M. Asada, T. Watanabe, T. Nagasu, K. Tsukahara, A. Iijima, K. Kitoh, Novel sulfonamides as potential, systemically active antitumor agents, J. Med. Chem. 35 (1992) 2496-2497.
14. K. Yoshimatsu, A. Yamaguchi, H. Yoshino, N. Koyanagi, K. Kitoh, Mechanism of action of E7010, an orally active sulfonamide antitumor agent: inhibition of mitosis by binding to the colchicine site of tubulin, Cancer Res. 57 (1997) 3208-3213.
15. Y. Liu, J. Wang, Y. Ji, G. Zhao, L. Tang, C. Zhang, X. Guo, Z. Liu, Design, synthesis, and biological evaluation of 1-methyl-1,4-dihydroindeno[1,2-c]pyrazole analogues as potential anticancer agents targeting tubulin colchicine binding site, J. Med. Chem. 59 (2016) 5341-5355.
16. J. Y. Mane, M. Klobukowski, Free energy calculations on the binding of colchicine and its derivatives with the α/β-Tubulin isoforms, J. Chem. Inf. Model 48 (2008) 1824-1832.
17. C. Tseng, J.Y Mane1, P.Winter, L. Johnson, T. Huzil, E. Izbicka, Quantitative analysis of the effect of tubulin isotype expression on sensitivity of cancer cell lines to a set of novel colchicine derivatives, Mol. Cancer 9 (2010) 131.
18. N. Sirisoma, A. Pervin, H. Zhang, S. Jiang, J. A. Willardsen, M.B. Anderson, G. Mather, C.M. Pleiman, S. Kasibhatla, B. Tseng, J. Drewe, S. Cai, Discovery of *N*-(4-methoxyphenyl)-*N*,2-dimethylquinazolin-4-amine, a potent apoptosis inducer and efficacious anticancer agent with high blood brain barrier penetration, J. Med. Chem. 52 (2009) 2341-2351.
19. S. Kasibhatla, V. Baichwal, S. Cai, B. Roth, I. Skvortsova, S. Skvortsov, P. Lukas, N. M. English, N. Sirisoma, J. Drewe, A. Pervin, B. Tseng, R. O. Carlson, C. M. Pleiman, MPC-6827: A small-molecule inhibitor of microtubule formation that is not a substrate for multidrug resistance pumps, Cancer Res. 67 (2007) 5865-5871.
20. A. Tsimberidou, W. Akerley, M. C. Schabel, D. S. Hong, C. Uehara, A. Chhabra, T. Warren, G. G. Mather, B. A. Evans, D. P. Woodland, E. A. Swabb, R. Kurzrock, Phase I clinical trial of MPC-6827 (azixa), a microtubule destabilizing agent, in patients with advanced cancer, Mol. Cancer Ther. 9 (2010) 3410-3419.
21. I. M. Subbiaha, D. J. Lenihanb, A. M. Tsimberidouc, Cardiovascular toxicity

profiles of vascular-disrupting agents, Oncologist 16 (2011) 1120-1130.

22. S. Banerjee, K. E. Arnst, Y. Wang, G. Kumar, S. Deng, L.Yang, G. Li, J. Yang, S.W. White, W. Li, D. D. Miller, Heterocyclic-Fused pyrimidines as novel tubulin polymerization inhibitors targeting the colchicine binding site: structural basis and antitumor efficacy, J. Med. Chem. 61(2018) 1704-1718.
23. X. Wang, F. Guan, E. Ohkoshi, W. Guo, L. Wang, D. Zhu, S. Wang, L. Wang, E. Hamel, D. Yang, L. Li, K. Qian, S. L. M. Natschke, S. Yuan, K. Lee, Lan Xie, Optimization of 4-(*N*-cycloamino)phenylquinazolines as a novel class of tubulin-polymerization inhibitors targeting the colchicine site, J. Med. Chem. 57 (2014) 1390-1402.
24. R. Devambatla, O. A. Namjoshi, S. Choudhary, E. Hamel, C. V. Shaffer, C. C. Rohena, S. L. Mooberry, A. Gangjee, Design, synthesis, and preclinical evaluation of 4-substituted-5-methyl-furo[2,3-d]pyrimidines as microtubule targeting agents that are effective against multidrug resistant cancer cells, J. Med. Chem. 59 (2016) 5752-5765.
25. H. Nara, K. Sato, T. Naito, H. Mototani, H. Oki, Y. Yamamoto, H. Kuno, T. Santou, N. Kanzaki, J. Terauchi, O. Uchikawa, M. Kori, Discovery of Novel, Highly Potent, and Selective Quinazoline-2-carboxamide-based matrix metalloproteinase (MMP)-13 inhibitors without a zinc binding group using a structure-based design approach, J. Med. Chem. 57 (2014) 8886-8902.
26. X. Deng, L. Guo, L. Xua, X. Zhen, k. Yu, W. Zhao, W. Fu, Discovery of novel potent and selective ligands for 5-HT2A receptor with quinazoline scaffold, Bioorg. Med. Chem. Lett. 25 (2015) 3970-3974.

Highlights:

- A series of quinazolines have been designed to occupy three zones of colchicine domain.
- **19c** showed the most potent *in vitro* anti-proliferative activity.
- **19c** was identified as a tubulin polymerization inhibitor with potent vascular disrupting activity.
- **19c** was validated to occupy three zones of colchicine domain on *in silico* studies.
- **19c** exhibited potent tumor growth inhibition in H22 liver cancer xenograft mouse model.

Graphic abstract

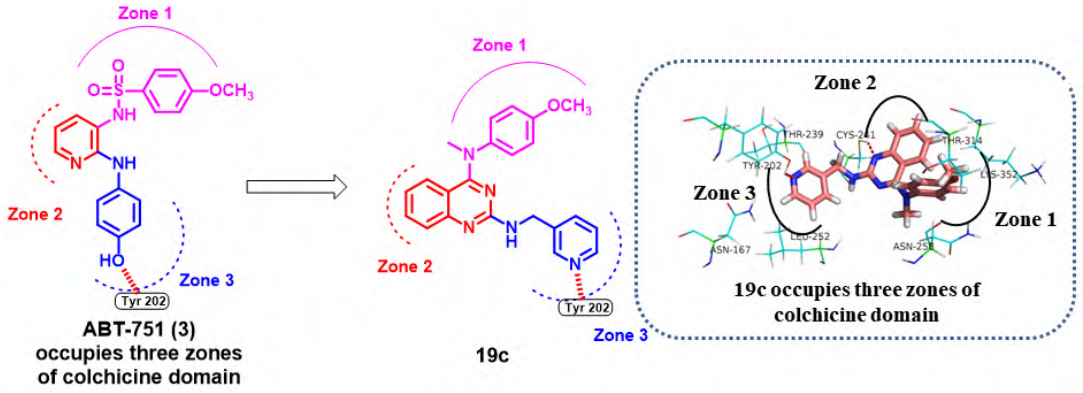

IPA: IC_{50} = 2.24 μM
Cytotoxicity: IC_{50} = 2.82 - 5.94 μM

IPA: IC_{50} = 2.45 μM
Cytotoxicity: IC_{50} = 0.10 - 0.13 μM

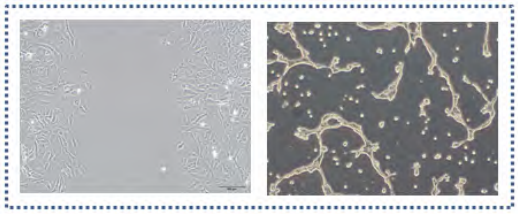

In vitro anti-vascular activity of 19c (0.2 μM)

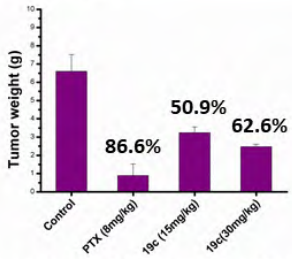

In vivo anti-tumor activity